PROCEEDINGS, 49th Workshop on Geothermal Reservoir Engineering
Stanford University, Stanford, California, February 12-14, 2024
SGP-TR-227

Preliminary Tectonic and Structural Controls of Geothermal Springs of the Tibetan Plateau: Insight from Regional-Scale Sampling of Helium-Isotopes ($^3He/^4He$), Stable Isotopes, and Aqueous Geothermometry

Jason W. Craig[1], Simon L. Klemperer[1,2], Laura J. Crossey[3], Karl E. Karlstrom[3], Ping Zhao (赵平)[4]

1. Department of Earth and Planetary Sciences, Stanford University, Stanford, CA 94305-2115
2. Department of Geophysics, Stanford University, Stanford, CA 94305-2215
3. Department of Earth and Planetary Sciences, University of New Mexico, Albuquerque, NM 87131
4. State Key Laboratory of Tibetan Plateau Earth System, Resources and Environment (TPESRE), Institute of Tibetan Plateau Research, Chinese Academy of Sciences, Beijing, China

Corresponding author: jwcraig@stanford.edu

Keywords: Tibet, fault, structure, helium isotopes, stable isotopes, geothermometry, geochemistry, tectonics

ABSTRACT

Geothermal activity is prolific across the Himalaya-Tibet orogen, yet the principal tectonic mechanism controlling upper-crust hydrothermal circulation across this region remains unresolved. We use regional-scale geochemical sampling of spring systems and integrate classical fluid geothermometry, helium ($^3He/^4He$) isotopes, and stable isotopes of water with the mapped distributions of active fault traces to characterize regional heat source(s) and permeability pathways for hydrothermal flow. We utilize helium-isotope measurements from 196 localities and aqueous chemistry along with stable isotope data from 142 springs, yielding a dataset of 127 spring systems with both isotopic and chemical analyses. Stable isotopes of water ($\delta^{18}O - \delta D$) cluster near the local meteoric water line for nearly all springs sampled across the Tibetan Plateau, demonstrating that there is minimal rock-water interaction and meteoric recharge is the principal source of fluids for geothermal reservoirs of the region. In total, 70% of springs in our database are recognized as likely being associated with active fault systems, and elevated temperatures are positively correlated with fault control. Fifty-seven springs (40% total) across the region yield quartz-geothermometry estimates >120°C, with four of those geothermal systems >180°C. Southern Tibet contains the greatest density of high-temperature geothermal systems (those for which quartz-geothermometry yields modeled temperatures >120°C), with model temperatures up to 215°C, that all have crustal $^3He/^4He$ ratios and are associated with major north-trending normal faults or conjugate northeast and northwest-striking strike-slip faults. Even the hottest springs in northern Tibet (quartz-geothermometry temperature of 152°C) are not as hot, but most of these high-temperature systems are located close to active northeast-striking strike-slip faults. Observed $^3He/^4He$ ratios are higher in northern Tibet, requiring some mantle volatile contribution. We attribute the principal control for geothermal systems in Tibet to be active extensional and transtensional fault zones that locally elevate permeability to allow deep (~8-14 km) circulation of aqueous solutions to mid-upper crustal depths across a region with normal-to-elevated heat flux.

1. INTRODUCTION

Tibet, also known as the "roof of the world" (average elevation ~4500 meters), is one of the most prolific geothermal provinces on Earth with abundant thermal springs, yet the geologic processes responsible for the geothermal activity remains unclear. Understanding the controlling physical properties for geothermal activity of the Tibetan Plateau has implications for the transmission of fluids and thermal structure of continent-continent orogens. Geothermal resources of the region can be harnessed by the isolated communities of Tibet as a reliable source of renewable power and direct heating, which are currently underutilized. Practically, targeting the structural controls for hydrothermal upwelling in the upper crust is key to minimizing risk in geothermal exploration programs.

Although the close association of geothermal manifestations in Tibet with active faults was recognized by Han (1984), most work has focused on the heat source for these geothermal systems, suggested to be circulation of topographically driven groundwater to upper crustal depths (<5 km) in continental crust with average-to-elevated heat flux (60 to 90 mW/m^2) (Hochstein and Yang, 1992), the presence of active intra-crustal magmatic systems (Xue et al., 2023; Yokoyama et al., 1999; Guo et al., 2019), or a combination of these two models (Tan et al., 2014). Conductive zones imaged by magnetotelluric surveys may lie above or below the ductile-brittle transition zone (~15 km) and are interpreted as crustal melts that may be acting as a source of heat and fluid for spatially correlated geothermal systems on the surface (Xue et al., 2023; Arora et al., 2007; Harinarayana et al., 2006). We consider these hypotheses using regional-scale geochemical sampling of spring systems and integrate classical fluid geothermometry, helium ($^3He/^4He$) isotopes, stable isotopes of water, and distribution of active fault traces to characterize regional heat source(s) and permeability pathways for hydrothermal flow in Tibet.

This study presents aqueous chemistry measurements collected during a sampling campaign for helium isotopes ($^3He/^4He$) of warm and hot springs across the Himalayan-Tibetan orogen (Figure 1; Klemperer et al., 2022). A 1,000-km-long helium boundary is interpreted to overlie the "mantle suture" where cold underplated Indian lithosphere is juxtaposed at >80 km depth (Fig. 1B) against a sub-Tibetan

incipiently molten asthenospheric mantle wedge and demonstrates limited underthrusting for the Tibetan continental collision. Evaluating paired helium isotope ($^3He/^4He$), stable isotope, and aqueous chemistry data in the context of neotectonics provides a unique opportunity to investigate the nature and origin of hydrothermal fluids across the entirety of the lithosphere of the Tibetan Plateau.

2. TECTONIC FRAMEWORK

The Himalayan ranges are composed of a series of active north-dipping thrust sheets (Yin and Harrison, 2000) that root into the Main Himalayan Thrust which projects to the surface as the Main Frontal Thrust (Fig. 1). North of this orogenic thrust wedge is the Tethyan Himalaya terrane (Fig. 1), a package of Indian continental-margin sedimentary rocks bounded to the south by the South Tibetan Detachment (STD) and to the north by the Yarlung-Zangbo suture (YZS). The YZS marks the ~57 Ma collision of the Indian and Eurasian plates (Leech et al., 2005). North of the YZS are the Lhasa, Qiangtang and Songpan-Ganzi terranes (Fig. 1), themselves bounded by east-west trending suture zones, but deforming today by upper-crustal rigid block rotation above lower-crustal channel flow (Thatcher et al., 2007; Zhang et al., 2004). Extension initiated along the east-west striking South Tibetan Detachment (Fig. 1) that developed in response to gravitational collapse (Burchfiel and Royden, 1985). Mid-Miocene to modern extension has resulted in active north-northeast-striking normal faults (Fig. 1) in southern and central Tibet (Yin and Harrison, 2000), perhaps driven by east-west directed channel flow in the deeper crust (Liu et al., 2014). The extent of deformation related to these modern rift systems is debated, as normal faulting may be limited to the brittle upper crust and developed in response to orogenic gravitational collapse (Burchfiel and Royden, 1985) or be lithospheric in scale (Liang et al., 2012; Yin, 2000). Conjugate northwest and northeast-striking strike-slip faults (Fig. 1) accommodate relative motion from both north-south crustal shortening and east-west extension (Gan et al., 2007), developing and interacting with normal faults in complex, intermeshed transtensional fault zones (Taylor and Yin, 2009, and references therein). The scale of deformation associated with major strike-slip faults is also contentious. For instance, different workers argue whether the Karakoram fault is restricted to the brittle upper crust (Phillips et al., 2004), or continues to the base of the lithosphere (Rolland et al., 2009). Active volcanism is limited to the northern Qiangtang and Songpan-Ganzi terranes (Fig. 1), and there is no evidence for volcanic rocks in central and southern Tibet younger than ~8 Ma (Guo and Wilson, 2019).

3. METHODS AND RESULTS

Fieldwork was completed over multiple years, sampling warm and hot springs following the catalog of Tong et al. (2000). In this work we utilize helium-isotope measurements from 196 localities and aqueous chemistry along with stable isotope data from 142 springs, yielding a dataset of 127 spring systems with both isotopic and chemical analyses (Fig. 1). Here we use major-element geochemistry of the surface discharge of geothermal springs to evaluate the degree of mixing of different waters and to estimate reservoir temperatures by solute geochemical geothermometry (Fig. 2). We use oxygen and deuterium isotope measurements from the springs to help constrain the origin of waters and the extent of water-rock interactions (Fig. 2b). Helium-isotope data provides insight into volatile sourcing related to mantle melting and degassing, or crustal alpha-particle production from radiogenic decay. Lastly, we evaluate structural controls for each spring with aqueous chemistry to determine the relationship between active faulting and temperature.

3.1 Aqueous Chemistry

Water chemistry analysis was completed at the University of New Mexico (UNM). Field parameters were measured for each location including pH, temperature (°C), and specific conductance (μS/cm). All sampling equipment (bottles, syringes, and filters) was rinsed with sample water three times prior to collection. Two bottles were collected at each location, an unfiltered raw sample of 125 ml for alkalinity, anion, and stable-isotope analysis and a filtered (0.45 μM) and acidified (HNO_3) sample of 60 ml for cation analysis. The 125 ml sample was collected with zero headspace to prevent degassing that could affect the alkalinity measurement in the lab.

Alkalinity was determined using the end-point titration method with 0.020 N sulfuric acid (H_2SO_4) and an Oakton pH/CON 300m in the Diagenesis Laboratory at UNM (Baird et al. 2017). Samples are titrated from the zero-headspace bottle as soon as possible following sample collection. Duplicate data showed an error of <2.0% for alkalinity. Anion samples are analyzed using ion chromatography (IC) and cation samples are analyzed using inductively coupled plasma optical emission spectrometry (ICP-OES) in the analytical geochemistry laboratory at UNM. Standard methods were used for IC (Jackson, 2000) and ICP-OES (Hou and Jones, 2000) comparable to US EPA 300.0 and EPA 200.7, respectively. Samples were diluted as needed when concentrations exceeded the standard of 20 ppm for anions or 10 ppm for cations. Ten percent duplicates were routinely run for all methods in addition to the quality assurance lab standards and blanks during analysis.

Stable-isotope analysis of hydrogen and oxygen was carried out using cavity ring-down spectroscopy (Picarro L1102-I) at the Center for Stable Isotopes, UNM. Isotope values are reported based on the ratio of the heavy to the light isotope such as $^{18}O/^{16}O$ for oxygen or $^2H/H$ (D/H) for hydrogen. Both oxygen and hydrogen isotopes are reported with respect to the Vienna Standard Mean Ocean Water (VSMOW). We used the standard calculation to report the isotope composition in delta notation (Sharp, 2017). The units for isotope composition are reported as parts per thousand (‰ or per mil) deviation from the standard. Each sample was analyzed six times and then averaged. Results show each sample to routinely be within an error of 0.1‰ for $\delta^{18}O$ and 2.0‰ for $^{\delta}D$. Duplicates were also run at a frequency of 10% and showed the same margins of error.

Springs across the Tethyan Himalaya, Lhasa, and Qiangtang terranes show a wide range of chemistry and generally overlap on ternary diagrams (Fig. 2A) indicating no major spatial trends in chemistry that are unique to terrane or lithology. Bicarbonate-type fluids predominate with a lesser proportion of sulfate and chlorite-type fluids. Stable isotopes of water ($\delta^{18}O$ – δD, Fig. 2B) cluster near the local meteoric water line (LMWL) of Tan et al. (2014), indicating that there is minimal rock-water interaction and meteoric recharge is

the principal source of fluids for nearly all the geothermal systems sampled across the Tibetan Plateau. Similarly, most springs plot in the immature water field of the Na-K-Mg ternary plot (Fig. 2C, Giggenbach, 1991), which agrees with the stable-isotope data, and only 26 springs (18%), mostly located in the Tethyan Himalaya and Lhasa terranes, lie in the partial-equilibration field. The majority of springs contain significant bicarbonate and plot in the peripheral water domain of the Cl-SO_4-HCO_3 ternary (Fig. 2D, Giggenbach, 1991), consistent with a meteoric origin for fluids.

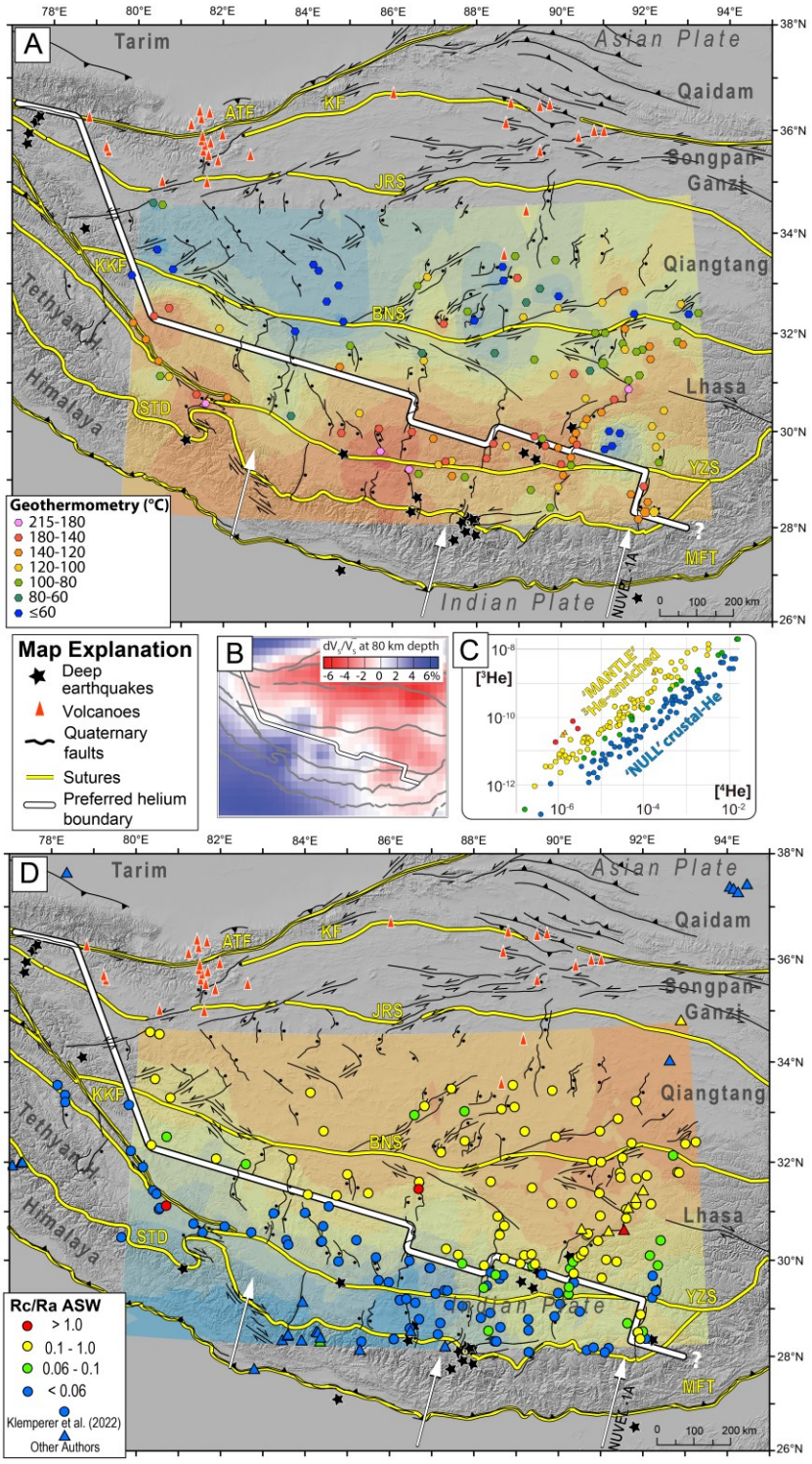

Figure 1: Sample locations with spring temperature and helium isotope ratios. (*A*) Aqueous geothermometry (quartz conductive) temperature (°C) estimates from sampled springs (temperature-colored circles), spatially interpolated, with

warmer colors indicating higher temperatures. Mantle suture: thin solid white line shows 10-km-wide helium boundary that separates "mantle" samples from "null" samples (shown in part D). Mantle suture is almost everywhere north of all 65-to-100-km deep earthquakes (black stars) and always south of Quaternary volcanoes (narrow red triangles) and is constrained to trend 105° orthogonal to plate-convergence vector (white arrows) and to be offset only at active faults (black lines, from Mohadjer et al., 2016). Yellow lines: sutures/major faults. MFT, Main Frontal thrust; STD, South Tibetan detachment; YZS, Yarlung–Zangbo suture; BNS, Banggong-Nujiang suture; JRS, Jinsha River suture; KF, Kunlun fault; ATF, Alyn Tagh fault; KKF, Karakoram Fault. (B) Seismic body-wave tomography, dVp/Vp at 80 km depth (Chen et al., 2017), same area as A and D, overlain by preferred helium boundary (white line). (C) Measured abundance of [^{3}He] vs. [^{4}He] color-coded as in map (D), showing bimodality with two parallel but clearly separated trend-lines. (D) ^{3}He/^{4}He isotope data (R_C/R_A); circles and triangles, color-coded red "mantle" samples >1R_A; yellow "mantle" samples >0.1R_A; green "intermediate" samples >0.06R_A; blue "null" samples ≤0.06R_A, on same map base as part A, with warmer colors indicating higher R_C/R_A. For additional data sources see Klemperer et al. (2022).

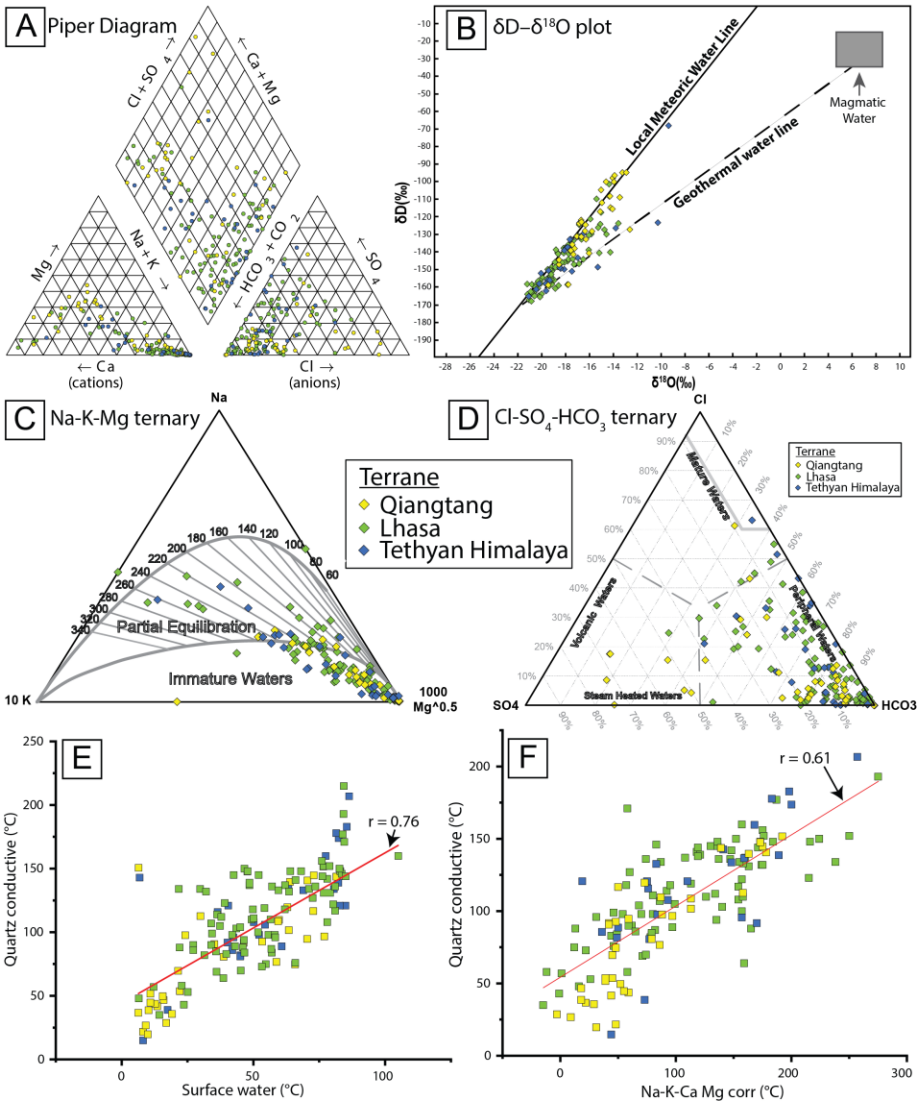

Figure 2: Spring temperatures and chemistry of Tibetan warm and hot springs. All plots have data colored based on terrane: Qiangtang, yellow; Lhasa, green; Tethyan Himalaya, blue. (*A*) Piper diagram of water samples (generated using GUI from Russoniello et al., 2020). (*B*) δD–δ^{18}O plot. The LMWL (δD = 8.0 × δ^{18}O + 14.4), and magmatic fluid distribution (δ^{18}O = 7 ± 2‰, δD = -25 ± 10‰) are from Tan et al., (2014). (*C*) Na-K-Mg ternary diagram. (*D*) Cl-SO_4-HCO_3 ternary anion plot. (*E*) Cross plot of measured surface temperature (°C) and quartz conductive geothermometry estimates (°C). (*F*) Cross plot of quartz conductive and Na-K-Ca Mg corrected geothermometry estimates (°C).

Aqueous geothermometry for reservoir-temperature estimates of springs used calculations provided by Powell and Cumming (2010). Measured surface spring temperatures, silica geothermometry, and cation geothermometry estimates are all well-correlated (Fig. 2E-F). We use the quartz conductive geothermometer (Fournier and Potter, 1982) as a standardized parameter hereafter for evaluating regional patterns of temperature variation in geothermal springs in relation to the regional tectonic setting (Fig. 1A), but we recognize that these are model temperatures, not a definitive measure of source temperatures, particularly for lower-temperature sources <150°C (the vast majority of our data).

Fifty-seven springs (40% total) across the region yield quartz-geothermometry estimates >120°C, with four of those geothermal systems >180°C. The Tethyan Himalaya and Lhasa terranes have a greater number of higher-temperature systems, and average geothermometer temperatures of 118°C and 115°C, respectively. In comparison, maximum (151°C) and average (85°C) estimated temperatures are lower in the Qiangtang terrane, and there is a greater number of cold geothermal systems (<80°C). Interpolation of quartz geothermometry estimates produces a contour map (Fig. 1A) demonstrating a broad region across the Tethyan Himalaya and Lhasa terranes with elevated temperatures of geothermal springs relative to lower temperatures in the Qiangtang terrane.

3.2 Helium isotopes ($^3He/^4He$)

[^{3}He] and [^{4}He] for each sample were measured at Scripps Institute for Oceanography and at the Ohio State University (Klemperer et al., 2022) (Fig. 1C) and corrected for atmospheric contributions, if any, using the He/Ne ratio of air-saturated water (ASW) at the actual temperature, elevation, and salinity of each spring [hereafter $(He/Ne)_{ASW,\ Field\ T}$]. We compare the ratio of corrected $^3He/^4He$ (= R_C) to the same ratio for air ($R_A = 1.384 \times 10^{-6}$) giving R_C/R_A (Fig. 1D). Samples with $R_C > 0.1\ R_A$ indicate the addition of mantle volatiles and are referred to as "mantle" samples. Samples with $0.06\ R_A < R_C \leq 0.1\ R_A$ are considered "intermediate," or include some component of mantle volatile sourcing. Samples with $R_C \leq 0.06\ R_A$ are termed as "null," or of crustal composition. The choice of cutoff values of 0.06 R_A and 0.1 R_A is supported by the bimodal distribution of sample values (Fig. 1C). A full discussion of our methods and helium-isotope results is presented in Klemperer et al. (2022).

Five springs have $R_C/R_A > 1.0$, which is considered an incontestable signal of recently added mantle volatiles, but only one of those springs (sample ZDX17 in Fig. 3B) is correlated with an unusually high model source temperature (~170°C). Helium isotopes in southern Tibet (here, Tethyan Himalaya and southern Lhasa block) are crustal (i.e. $R_A/R_C < 0.06$), demonstrating that these geothermal systems lack any mantle volatile source. $^3He/^4He$ ratios are higher in northern Tibet (here, northern Lhasa block and Qiangtang), 0.1–1 R_C/R_A, requiring some mantle volatile contribution, and limited Quaternary volcanism is present albeit north of our spring coverage (Fig. 1).

3.3 Structural analysis

Faulting can increase the permeability of rocks through the propagation of open fractures in the core and damage zone of a fault (Caine et al., 1996). The relationship between active faults and geothermal springs included in this study was principally evaluated using the Central Asia Quaternary fault database of Mohadjer et al. (2016) (Figs. 1 and 3). Due to the regional scale of mapping and potential for thermal springs manifesting on the surface as outflow after traveling significant distances from the zone of upflow, a 15-km buffer (Fig. 3A) was applied to mapped fault traces before evaluating the relationship of springs relative to active faults. The buffer accounts for uncertainty in both fault-trace location and secondary structures (blind and unmapped) surrounding major fault zones. This metric does not account for hot springs controlled by blind faults or unmapped faults in areas with substantial topographic relief.

We identified 70 springs (~50% of all the localities sampled with aqueous-chemistry measurements) within the 15-km buffer. All spring localities were evaluated for fault control (e.g., offset alluvial surfaces and bedrock exposures) using remote sensing (Google Earth satellite imagery) as an additional metric for evaluating fault control. An additional 29 springs not captured in the 15-km fault buffer were identified as being associated with faults that are not included in the regional Quaternary fault dataset, using Google earth imagery, and these faults potentially have significant permeability associated with recent fault motion. In total, we recognize 99 springs (70% total) as likely being associated with active fault systems. Average quartz-geothermometry estimates are 23% hotter for springs with fault control than for springs without confirmed fault control. In the Qiangtang terrane, average quartz-geothermometry estimates are elevated by 32°C for fault-controlled springs. We attempted to further evaluate structural control on hydrothermal flow by examining strain-rate values (Kreemer et al., 2014), but found only a slight positive correlation with model temperatures.

Specific fault geometries and structural settings are known to be related to fracture-dominated permeability along fault systems, resulting in localized conduits for channeling upwelling hydrothermal fluids (Curewitz and Karson, 1997; Faulds et al., 2006, 2011, 2013; Siler et al., 2018). For each spring where fault control was established, we assessed and catalogued the structural setting using the terminology of Faulds and Hinz (2015) (Fig. 3B–E). Globally, most developed geothermal systems (75+) worldwide in andesitic arcs are in extensional and transtensional settings (intra-arc) (Moeck, 2014; Hinz et al. 2016), and this pattern of fault-related deformation is repeated in Tibet as anticipated from dominant focal mechanisms on the Tibet Plateau (Bai et al., 2017). The most common type of structural settings for hot springs we sampled in Tibet are fault terminations (20%), fault bends (20%), hybrid settings (15%), displacement transfer zones (14%), and pull aparts (9%). Transtensional structural settings dominate the Qiangtang and Tethyan Himalaya, whereas fault bends and terminations along major normal faults are the most common settings for the Lhasa terrane. Undetermined structural settings are common in the Tethyan Himalaya region (38%) where dramatic relief obscures complexities in fault geometry.

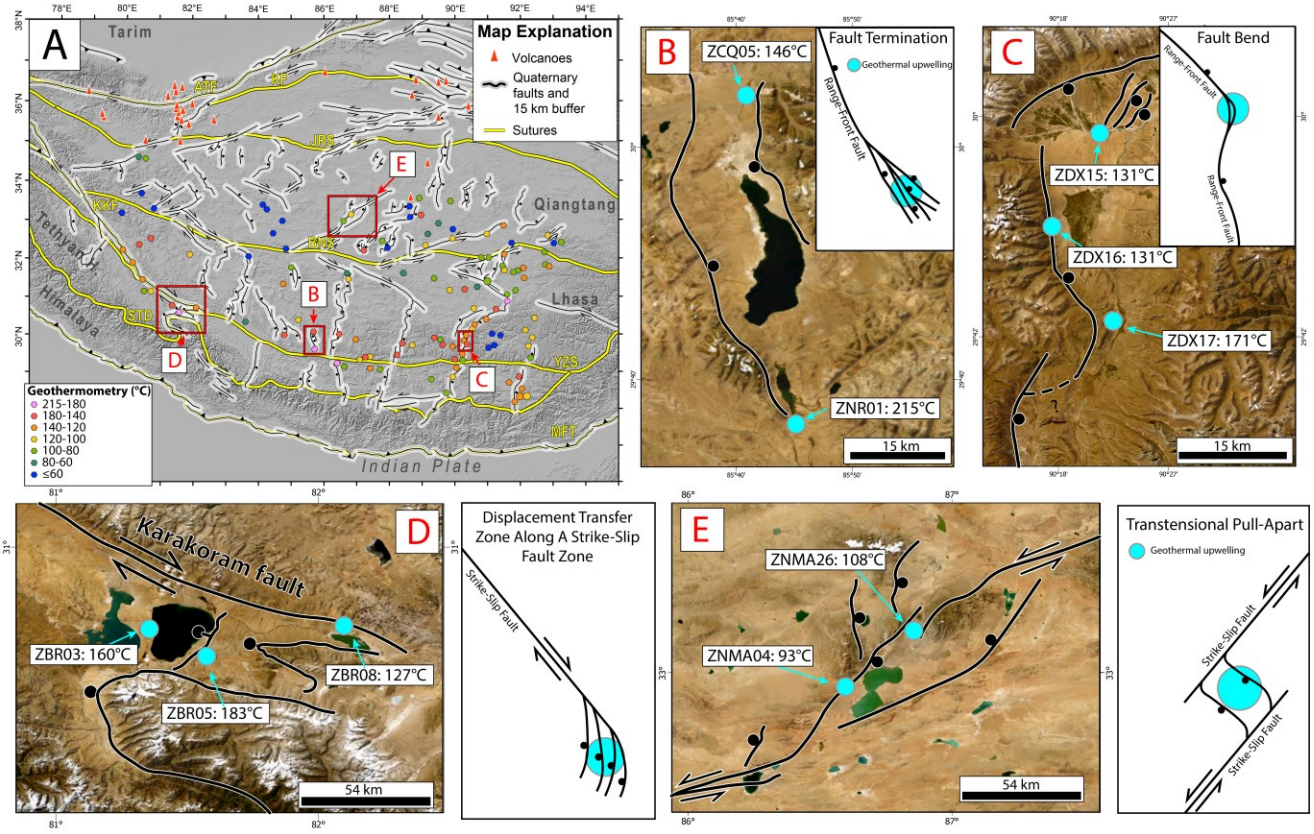

Figure 3: Structural controls for geothermal springs of Tibet and example favorable structural settings. (*A*) Mapped active fault traces (black lines) of Tibet (Mohadjer et al., 2016) with 15 km buffer (wide white lines) and springs color-coded by quartz-geothermometry temperatures. Locations of insets *B-E* shown as red rectangles. (*B-E*) Example hot springs with fault geometries typical of favorable structural settings for known geothermal systems, Basin-and-Range Province (Faulds et al. 2011). Cartoons depict faults (black lines) as principal control of zones of geothermal upwelling (cyan dots). Satellite imagery is overlain with active faults (from part A) and spring locations (cyan dots) labeled with sample ID and quartz geothermometry temperature estimates. (*B*) Fault-termination structural setting along the Dong Co conjugate fault system. (*C*) Fault-bend structural setting in the Yangbajain graben. Northern edge of map is ~3km south of the Yangbajain geothermal powerplant. (*D*) Displacement transfer zone along the southern margin of the right-lateral Karakoram fault. (*E*) Transtensional pull-apart along the left-lateral Riganpei Co fault system.

4. DISCUSSION

Southern Tibet (defined here as south of the central region of the Lhasa terrane) contains the greatest density of high-temperature (>120 °C) quartz geothermometry estimates (Fig. 1A), almost all with crustal $^{3}He/^{4}He$ ratios (Fig. 1B), and generally located in proximity to major north-south striking normal faults or conjugate strike-slip faults (Fig. 3A). Springs north of the helium boundary line yield fewer high-temperature geothermometry estimates (Fig. 1A), but most of the associated springs are located close to active faults (Figs. 3 and 4). Observed $^{3}He/^{4}He$ ratios are higher in northern Tibet (Fig. 1B), 0.1–1 R_C/R_A, requiring some mantle volatile contribution, and limited Quaternary volcanism is present albeit north of our sample coverage (Fig. 1).

The greater density of high-temperature geothermal systems in our southern area is suggestive of higher upper-crustal heat flow than in our northern area. This thermal contrast is opposite to that understood in the deep crust, where cold underplated Indian lithosphere underlies southern Tibet but an asthenospheric mantle wedge underlies northern Tibet (Fig. 1B) (Craig et al., 2020; Klemperer et al., 2022). Results from aqueous geochemistry and stable isotopes of water indicate that hydrothermal fluids across the Tibetan Plateau are primarily derived from meteoric sources. Fluids transmitted from the mid-lower crust make up a negligible portion of the total fluid budget reaching the surface, which is consistent with empirical measurements that predict minimal permeability across the ductile-brittle transition zone (Violay et al., 2017).

Helium-isotope results and substantial mixing of meteoric fluids support an amagmatic, mid- to upper-crustal heat source for the geothermal activity in southern Tibet. Regional extensional exhumation since the Miocene (Xu et al., 2024; Bian et al., 2022) has likely contributed to the elevated geothermal gradient for southern Tibet (Hu et al., 2000) and the associated widespread geothermal activity.

In comparison, extension and geothermal activity in northern Tibet is not as well developed, and high-temperature geothermal systems appear to be associated with major strike-slip faults that are tapping deeper, possibly mantle-derived fluids. Nevertheless, amagmatic fault-controlled circulation within the upper-crust is also the main mechanism for geothermal activity of northern Tibet, and regional geothermal gradients for this region are likely lower than in southern Tibet.

We attribute the principal control for geothermal systems in Tibet to be active, dilatational fault zones that locally elevate permeability to allow deep (~8-14 km) circulation of water to mid-upper crustal depths across this region with elevated heat flow, particularly in favorable extensional and transtensional structural settings (Fig. 3B-E). Fault-controlled hydrothermal flow from these depths does not require the presence of crustal melts as a heat source for the high-enthalpy geothermal systems and is assisted by the effect of topographically driven groundwater circulation. The presence of crustal melts in most of the upper crust of southern and central Tibet remains speculative. Where magmatic controls are present (Jaupart et al., 1985; Makovsky and Klemperer, 1999; Klemperer, 2006) the pathways for fluid and magma ascent are still significantly localized along active fault systems (e.g. strike-slip fault systems of northern Tibet; Yin and Taylor, 2009). The presence of crustal melts below the ductile-brittle transition (DBT) zone would locally increase heat flow, but the contribution of fluids across the DBT is expected to be insufficient to term such systems as "magmatic," as active faults are still the primary control for channeling upwelling thermal convection. These systems are better characterized as amagmatic and fault-controlled. Primary rock permeability is likely not sufficient to circulate fluids to depths >3-6 km (Frisbee et al., 2017) as required for the observed high-temperature geothermal systems if topographically driven groundwater circulation is the only mechanism at play. Thus, secondary fault-induced permeability is necessary to sustain elevated flow rates for rapid transmission of hot, unequilibrated, meteoric fluids through the upper crust.

Application of structurally based exploration strategies that have been successful in extensional to transtensional amagmatic tectonic settings (e.g. Craig et al., 2021) may aid in the future targeting and development of the geothermal resources of Tibet. Furthermore, Tibet might have significant blind geothermal resources as in other amagmatic geothermal provinces where blind geothermal systems represent the bulk of total geothermal resources (e.g. Basin-and-Range Province, Coolbaugh et al., 2006). Exploration for blind geothermal systems may provide alternative sources of renewable power in areas where geothermal activity was previously considered insufficient or nonexistent for development, particularly near isolated communities in need of reliable sources of energy and direct heating.

5. CONCLUSIONS

Measured surface temperatures and aqueous geothermometry suggest the Himalayan-Tibet orogen is a region with elevated heat flow. Warm and hot springs are distributed across a broad area lacking any surface Quaternary volcanism. Spring temperatures, and model quartz-geothermometry temperature estimates for the associated spring systems, are greater in southern Tibet than in northern Tibet, which requires a north-to-south increase in upper-crustal heat flow. An opposite relationship is likely present in the thermal structure of the deep lithosphere (>80 km depth) as higher temperatures are present in northern Tibet where there is a sub-Tibetan incipiently molten asthenospheric mantle wedge and lower temperatures are present in southern Tibet due to the presence of cold underplated Indian lithosphere. Nearly all warm and hot springs across the Tibetan Plateau derive their fluids from meteoric sources and there is no correlation between the presence of mantle-derived volatiles and spring temperatures. Fluids transmitted across the ductile-brittle transition make up a negligible portion of the total hydrothermal fluid budget reaching the surface. We propose that amagmatic active fault systems are the principal geologic controls for the geothermal activity of Tibet. Complex extensional and transtensional tectonics of the region increase permeability in a region with elevated heat flow and enable rapid, deep circulation of meteoric fluids to mid-upper crustal depths. Structurally focused exploration programs in similar tectonic settings have yielded successful results for targeting zones of hydrothermal upflow and this strategy is recommended for the future exploration of the abundant geothermal resources of Tibet.

REFERENCES

Arora, B. R., Unsworth, M. J., and Rawat, G.: Deep resistivity structure of the northwest Indian Himalaya and its tectonic implications, Geophysical Research Letters, 34, (2007), L04307, doi:10.1029/2006GL029165.

Bai, L., Li, G., Khan, N.G., Zhao, J., Ding, L.: Focal depths and mechanisms of shallow earthquakes in the Himalayan–Tibetan region, Gondwana Research, v. 41, (2017), 390-399, https://doi.org/10.1016/j.gr.2015.07.009.

Bian, S., Gong, J., Zuza, A. V., Yang, R., Chen, L., Ji, J., Yu, X., Yian, Y., Cheng, X., Lin, X., Chen, H.: Along-strike variation in the initiation timing of the north-trending rifts in southern Tibet as revealed from the Yadong-Gulu rift, Tectonics, 41, (2022), e2021TC007091. https://doi.org/10.1029/2021TC007091

Baird, R.B., Eaton, A.D., Rice, E.W.: Standard methods for the examination of water and wastewater, 23rd edition. American Public Health Association, Washington, DC, (2017).

Burchfiel, B. C., and Royden, L. H.: North-south extension within the convergent Himalayan region. Geology, 13(10), (1985), 679-682.

Caine, J.S., Evans, J.P., Forster, C.B.: Fault zone architecture and permeability structure. Geology, 24, (1996), 1025–1028. https://doi.org/10.1130/0091-7613(1996)

Chen, M., Niu, F., Tromp, J., Lenardic, A., Lee, C.A., Cao, W., and Ribeiro, J.: Lithospheric foundering and underthrusting imaged beneath Tibet, Nature Communications, 8, (2017), 15659. https://doi.org/10.1038/ncomms15659

Coolbaugh, M.F., Raines, G.L., Zehner, R.E., Shevenell, L., Williams, C.F.: Prediction and discovery of new geothermal resources in the Great Basin: multiple evidence of a large undiscovered resource base, Geothermal Resources Council Transactions, 30, (2006), 867–874.

Craig, J.W., Faulds, J.E., Hinz, N.H., Earney, T.E., Schermerhorn, W.D., Siler, D.L., Glen, J.M., Peacock, J., Coolbaugh, M.F., Deoreo, S.B.: Discovery and Analysis of a Blind Geothermal System in Southeastern Gabbs Valley, 97, Geothermics, western Nevada, USA (2021), p. 18, 10.1016/j.geothermics.2021.102177

Craig, T. J., Kelemen, P. B., Hacker, B. R., and Copley, A.: Reconciling geophysical and petrological estimates of the thermal structure of southern Tibet, Geochemistry, Geophysics, Geosystems, 21, (2020), e2019GC008837. https://doi.org/10.1029/2019GC008837

Curewitz, D., Karson, J.A.: Structural settings of hydrothermal outflow: fracture permeability maintained by fault propagation and interaction. Journal of Volcanology and Geothermal Research., 79, (1997), 149–168. https://doi.org/10.1016/S0377-0273(97)00027-9.

Faulds, J.E., and Hinz, N.H.: Favorable tectonic and structural settings of geothermal systems in the Great Basin region, western USA. In: Proxies for Discovering Blind Geothermal Systems: World Geothermal Congress 2015, (2015), Melbourne, Australia, p. 6.

Faulds, J.E., Hinz, N.H., Dering, G.M., and Siler, D.L.: The hybrid model — the most accommodating structural setting for geothermal power generation in the Great Basin, western USA. Geothermal Resources Council Transactions, 37, (2013), 3–10.

Faulds, J.E., Hinz, N.H., Coolbaugh, M.F., Cashman, P.H., Kratt, C., Dering, G., Edwards, J., Mayhew, B., and McLachlan, H.: Assessment of favorable structural settings of geothermal systems in the Great Basin, western USA. Geothermal Resources Council Transactions, 35, (2011), 777–783.

Faulds, J.E., Coolbaugh, M.F., Vice, G.S., and Edwards, M.L.: Characterizing structural controls of geothermal fields in the northwestern Great Basin: a progress report. Geothermal Resources Council Transactions, 30, (2006), 69–76.

Fournier R.O. and Potter R.W. II.: A revised and expanded silica (quartz) geothermometer, Geothermal Resources Council Bulletin, 11, (1982), 3-12.

Frisbee, M. D., D. G. Tolley, and J. L. Wilson.: Field estimates of groundwater circulation depths in two mountainous watersheds in the western U.S. and the effect of deep circulation on solute concentrations in streamflow, Water Resources Research, 53, (2017), 2693–2715, doi:10.1002/2016WR019553.

Gan, W., Zhang, P., Shen, Z.-K., Niu, Z., Wang, M., Wan, Y., Zhou, D., Cheng, J.: Present-day crustal motion within the Tibetan Plateau inferred from GPS measurements, Journal of Geophysical Research, 112, (2007), p. B08416

Giggenbach, W.F.: Chemical techniques in geothermal exploration: in UNITAR/UNDP Guidebook: Application of geochemistry in resources development, (1991), 119-144.

Guo, Q.H., Planer-Friedrich, B., Liu, M.L., Yan, K.T., Wu, G.: Magmatic fluid input explaining the geochemical anomaly of very high arsenic in some southern Tibetan geothermal waters, Chemical Geology, 513, (2019), 32–43. https://doi.org/10.1016/j.chemgeo.2019.03.008.

Guo, Z., and Wilson, M.: Late Oligocene-Miocene transformation of postcollisional magmatism in Tibet, Geology, 47(8), (2019), 776-780. https://doi.org/10.1130/G46147.1

Han, T.: The Fundamental Characteristics of Active Tectonics in Tibet (in Chinese), Geology in China, (1984), 12:21-24

Harinarayana, T., Azeez, K. A., Murthy, D. N., Veeraswamy, K., Rao, S. E., Manoj, C., and Naganjaneyulu, K.: Exploration of geothermal structure in Puga geothermal field, Ladakh Himalayas, India by magnetotelluric studies. Journal of Applied Geophysics, 58(4), (2006), 280-295.

Hinz, N., Coolbaugh, M., Shevenell, L., Stelling, P., Melosh, G., Cumming, W.: Favorable structural–tectonic settings and characteristics of globally productive arcs, Proceedings, 41st Workshop on Geothermal Reservoir Engineering. Stanford University, Stanford, California February 22–24, 2016. 8 pp.

Hochstein, M. P., and Yang, Z.: Modelling of terrain-induced advective flow in Tibet: Implications for assessment of crustal heat flow, In Proceedings of the 17th workshop on geothermal reservoir engineering, Stanford, CA, SGP-TR-141, (1992), p. 153-157.

Hou, X., Jones, B.T.: Inductively coupled plasma/optical emission spectroscopy, Encyclopedia of Analytical Chemistry: 9468–9485. (2000), https:// doi. org/ 10. 1002/ 97804 70027 318. a5110. pub3

Hu, S., He, L., and Wang, J.: Heat flow in the continental area of China: a new data set, Earth and Planetary Science Letters, 179(2), (2000), 407-419.

Jackson, P.E.: Ion chromatography in environmental analysis, Encyclopedia of analytical chemistry: 2779–2801. (2000), https:// doi.org/ 10. 1002/ 97804 70027 318. a0835

Jaupart, C., Francheteau, J. and Shen, X.J.: On the thermal structure of the southern Tibetan crust, Geophysical Journal of the Royal Astronomical Society, 81, (1985), 131-155. https://doi.org/10.1111/j.1365-246X.1985.tb01355.x

Klemperer, S.L., Zhao, P., Whyte, C.J., Darrah, T.H., Crossey, L.J., Karlstrom, K.E., Liu, T., Winn, C., Hilton, D.R., and Ding, L.: Limited underthrusting of India below Tibet: $^{3}He/^{4}He$ analysis of thermal springs locates the mantle suture in continental collision, Proceedings of the National Academy of Sciences, 119, (2022), e211387

Klemperer, S. L.: Crustal flow in Tibet: geophysical evidence for the physical state of Tibetan lithosphere, and inferred patterns of active flow, Geological Society, London, Special Publications, 268(1), (2006), 39-70.

Kreemer, C., Blewitt, G. & Klein, E. C.: A geodetic plate motion and Global Strain Rate Model, Geochemistry, Geophysics, Geosystems, 15, (2014), 3849–3889, geodesy.unr.edu/GSRM/v2.2/GSRM_strain.txt.Z last accessed 07/26/2021.

Leech, M. L., Singh, S., Jain, A. K., Klemperer, S. L., and Manickavasagam, R. M.: The onset of India–Asia continental collision: early, steep subduction required by the timing of UHP metamorphism in the western Himalaya, Earth and Planetary Science Letters, 234(1), (2005), 83-97.

Liang, X., Sandvol, E., Chen, Y. J., Hearn, T., Ni, J., Klemperer, S., Shen, Y., and Tilmann, F.: A complex Tibetan upper mantle: A fragmented Indian slab and no south-verging subduction of Eurasian lithosphere, Earth and Planetary Science Letters, 333, (2012), 101-111.

Liu, Q. Y., van der Hilst, R. D., Li, Y., Yao, H. J., Chen, J. H., Guo, B., Hua, S., Wang, J., Huang, H., and Li, S. C.: Eastward expansion of the Tibetan Plateau by crustal flow and strain partitioning across faults, Nature Geoscience, 7(5), (2014), 361-365.

Makovsky, Y. and Klemperer, S.L.: Measuring the seismic properties of Tibetan bright spots: Evidence for free aqueous fluids in the Tibetan middle crust, Journal of Geophysical Research, 104(B5), (1999), 10795-10825

Moeck, I.: Catalog of geothermal play types based on geologic controls, Renewable and Sustainable Energy Reviews, 37, (2014), 867-882, https://doi.org/10.1016/j.rser.2014.05.032.

Mohadjer, S., Ehlers, T. A., Bendick, R., Stübner, K., and Strube, T.: A Quaternary fault database for central Asia, Natural Hazards and Earth System Sciences, 16, (2016), 529–542, https://doi.org/10.5194/nhess-16-529-2016

Phillips, R. J., Parrish, R. R., and Searle, M. P.: Age constraints on ductile deformation and long-term slip rates along the Karakoram fault zone, Ladakh, Earth and Planetary Science Letters, 226(3), (2004), 305-319.

Powell, T., and Cumming, W.: Spreadsheets for geothermal water and gas geochemistry, In: Proceedings 35th Workshop on Geothermal Reservoir Engineering. Stanford University. Stanford, California, USA. (2010), https://pangea.stanford.edu/ERE/pdf/IGAstandard/SGW/2010/powell.pdf

Rolland, Y., Mahéo, G., Pecher, A., and Villa, I. M.: Syn-kinematic emplacement of the Pangong metamorphic and magmatic complex along the Karakorum Fault (N Ladakh), Journal of Asian Earth Sciences, 34(1), (2009), 10-25.

Russoniello, C.J., and LK Lautz.: Pay the PIED Piper: Guidelines to visualize large geochemical datasets on Piper Diagrams, Groundwater, 58(3), (2020), 464-469. doi: http://10.1111/gwat.12953

Sharp, Z.: Principles of Stable Isotope Geochemistry, 2nd Edition. (2017).

Siler, D.L., Hinz, N.H., and Faulds, J.E.: Stress concentrations at structural discontinuities in active fault zones in the western United States: implications for permeability and fluid flow in geothermal fields, Geologic Society of America Bulletin, 130, (2018), 1273–1288. https://doi.org/10.1130/B31729.1.

Tan, H., Zhang, Y., Zhang, W., Kong, N., Zhang, Q., and Huang, J.: Understanding the circulation of geothermal waters in the Tibetan Plateau using oxygen and hydrogen stable isotopes, Applied Geochemistry, 51, (2014), 23–32.

Taylor, M., and Yin, A.: Active structures of the Himalayan-Tibetan orogen and their relationships to earthquake distribution, contemporary strain field, and Cenozoic volcanism, Geosphere, 5 (3), (2009), 199–214. doi: https://doi.org/10.1130/GES00217.1

Tong, W., Liao Z., Liu S., Zhang Z., You M., and Zhang M.: Thermal Springs in Tibet (in Chinese), (2000) Beijing, Science Press, pp. 300. ISBN 7-03-007521-8.

Violay, M., Heap, M.J., and Acosta, M.: Porosity evolution at the brittle-ductile transition in the continental crust: Implications for deep hydro-geothermal circulation, Scientific Reports, 7, (2017), 7705. https://doi.org/10.1038/s41598-017-08108-5

Xu, T., Li, Y., Stuart, F.M., Ma, Z., Bi, W., Jia, Y., and Yang, B.: Assessing the activity of eastern Himalayan extensional structures: Evidence from low-temperature thermochronology of granitic rocks from Yadong, Minerals, 14(1): 66. (2024), https://doi.org/10.3390/min14010066

Xue, G., Chen, W., Zhao, P., Ren, W., He, Y., Lv, P., Lei, K., Zhao, Y.: Three-dimensional electrical structure model of the Yangbajain geothermal field in Tibet: Evidence obtained from magnetotelluric data, Science China Earth Sciences, 66(8), (2023), 1839–1852. https://doi.org/10.1007/s11430-002-1099-4.

Yin, A., and Harrison, T. M.: Geologic evolution of the Himalayan-Tibetan orogen, Annual Review of Earth and Planetary Sciences, 28(1), (2000), 211-280.

Yokoyama, T., Nakai, S.I., and Wakita, H.: Helium and carbon isotopic compositions of hot spring gases in the Tibetan Plateau, Journal of Volcanology and Geothermal Research, 88 (1–2), (1999), 99–107. https://doi.org/10.1016/S0377-0273(98)00108-5.